Log-Polar Based Scheme for Revealing Duplicated Regions in Digital Images

Qiumin Wu, Shuozhong Wang, and Xinpeng Zhang

***Abstract*—Region duplication is a common type of digital image tampering. This paper presents a log-polar based approach to detect such forgery even if the copied area has been rotated and/or scaled. We compute log-polar fast Fourier transform (LPFFT) on image blocks to approximate the log-polar Fourier transform (LPFT). LPFFT is based on a nearly log-polar system where conversion to log-polar coordinates only involves 1-D Fourier transform and interpolation operations. In addition to rotation and scaling invariance, computation complexity of LPFFT is $O(n^2 \log n)$, much lower than $O(n^4)$ of LPFT when n is large. Similarity of the LPFFT results between different blocks provides indication of image tampering. Experimental results show efficacy of the proposed method.**

***Index Terms*—Image forensics, pseudo log-polar transform, regional duplication detection, rotation and scaling invariance.**

I. Introduction

A common type of image manipulation is to clone one part of the image to another in the same image, known as *region duplication* or *copy-move*. Detecting region duplication is based on the presence of duplicated regions in the image. Some published methods are based on lexicographic sorting of quantized DCT coefficients of image blocks [1] or PCA of fix-sized image blocks [2]. However, region duplication is often accompanied with re-scaling and rotation as shown in Fig. 1. In such cases, the above methods will fail because image features such as eigenvalues of PCA bases and DCT coefficients change when the region is geometrically distorted (rotated and scaled). Bashar *et al.* [3] propose a method using DWT and kernel-PCA. These methods can detect copied regions that are flipped or rotated, but not re-scaled.

To solve the problem, rotation/scaling invariant features are used in image forensics [4]–[6], [16]. In [6], log-polar Fourier transform (LPFT) is performed on inscribed circles of image blocks, and cross-power spectrum used for correlation analysis. High computation complexity is a drawback of this method. Fourier–Mellin transform (FMT) is computed on image blocks in [4]. The resulting magnitude is projected to a 1-D descriptor to reduce complexity, but this limits applicability of the algorithm as it cannot detect forgeries with rotation of more than 10°. In [16], 1-D log-polar descriptor is also used to reduce computation cost. However, since log-polar grid points are located at intersections of radial lines and concentric circles, interpolation from the Cartesian system to a log-polar grid is needed. This causes considerable errors and reduces accuracy when the image's resolution is low or the block-size is small. In addition, scale invariant feature transform (SIFT) is used to extract rotation/scaling invariant features [5], but it may fail when the tampered region is small or lacks reliable SIFT points.

(a) (b)

Fig. 1. Object duplication with rotation and scaling: (a) original image and (b) temped image, in which an added bird is copied from another after 15° rotation and 80% size-reduction.

In this letter, we develop an improved method to detect duplicated regions in an image by using log-polar fast Fourier transform (LPFFT), which can tolerate rotation and scaling and has relatively low computation complexity. The method is based on modification of the pseudo-polar fast Fourier transform (PPFFT) [7]. Further, we improve the related works [8] and [9], compute LPFT on a nearly log-polar grid, and make conversion to log-polar coordinates solely by using 1-D Fourier transform and interpolation. Similarity between the source and target regions, even though geometrically adjusted, is exposed by comparing correlations of the LPFFT results.

II. LPFT and Implementing Problems

LPFT includes two steps: log-polar mapping and Fourier transform. Consider a source image $\mathbf{S}$ and its rotated/scaled replica $\mathbf{R}$ with a rotation angle θ_0 and scaling factor λ_0. Let f and g represent luminance values in $\mathbf{S}$ and $\mathbf{R}$ respectively:

$$f(x_{\mathrm{R}}, y_{\mathrm{R}}) = g\left[\lambda_0(x_{\mathrm{S}}\cos\theta_0 - y_{\mathrm{S}}\sin\theta_0), \lambda_0(x_{\mathrm{S}}\sin\theta_0 + y_{\mathrm{S}}\cos\theta_0)\right]. \quad (1)$$

In the log-polar coordinates, sample values of $\mathbf{S}_{\mathrm{LP}}$ and $\mathbf{R}_{\mathrm{LP}}$ are

$$\mathbf{R}_{\mathrm{LP}}(\rho_{\mathrm{R}}, \theta_{\mathrm{R}}) = \mathbf{S}_{\mathrm{LP}}(\rho_{\mathrm{S}} + \log\lambda_0, \theta_{\mathrm{S}} + \theta_0). \quad (2)$$

Manuscript received May 25, 2011; revised July 20, 2011; accepted July 26, 2011. Date of publication August 04, 2011; date of current version August 22, 2011. This work was supported by the Natural Science Foundation of China (60872116, 60832010), and by the Graduate Innovation Foundation of Shanghai University (SHUCX112111). The associate editor coordinating the review of this manuscript and approving it for publication was Dr. Athanassios Skodras.

The authors are with School of Communication & Information Engineering, Shanghai University, Shanghai 200072, China (e-mail: rynax_ls@shu.edu.cn; shuowang@shu.edu.cn; xzhang@shu.edu.cn).

Color versions of one or more of the figures in this paper are available online at http://ieeexplore.ieee.org.

Digital Object Identifier 10.1109/LSP.2011.2163507

From (2), $\mathbf{R}_{\mathrm{LP}}$ is a translated version of $\mathbf{S}_{\mathrm{LP}}$. Taking Fourier transform of both sides:

$$F_{\mathrm{R}}(u,v) = F_{\mathrm{S}}(u,v)\exp\left[2\pi j(u\log\lambda_0 + v\theta_0)\right]. \quad (3)$$

The subscript LP of $\mathbf{R}$ and $\mathbf{S}$ is omitted here. This equation indicates that $|F_{\mathrm{R}}| = |F_{\mathrm{S}}|$. In other words, Fourier transforms of $\mathbf{S}_{\mathrm{LP}}$ and its translated version, $\mathbf{R}_{\mathrm{LP}}$, differs only in phase. Thus, similarity of the contents in $\mathbf{S}$ and $\mathbf{R}$ can be measured with the quantity below, termed the *normalized cross power spectrum* of $\mathbf{S}$ and $\mathbf{R}$, which is a 2-D complex sinusoid:

$$G(u,v) = \frac{F_{\mathrm{R}}(u,v)F_{\mathrm{S}}^{*}(u,v)}{|F_{\mathrm{R}}(u,v)F_{\mathrm{S}}^{*}(u,v)|} = \exp\left[-2\pi j(u\log\lambda_0 + v\theta_0)\right]. \quad (4)$$

Inverse Fourier transform of a sinusoid is a delta function. Thus, a peak exists in the inverse Fourier transform, $\mathcal{F}_G^{-1}(u,v)$, if $\mathbf{R}$ is a rotated/scaled version of $\mathbf{S}$. An alternative way to describe content similarity is to use the *normalized gradient correlation* (NGC) [10], which can also recover rotation and scaling. However, NGC has ambiguity between θ_0 and $(\theta_0 \pm \pi)$ as mentioned in [10] and [11].

A major drawback of LPFT is high computation complexity that is $O(m^2n^2)$ for an $m \times n$ image. Although one can compute FFT on the Cartesian grid and then interpolate the results to the polar grid, this introduces large interpolation errors [12]. Liu *et al.* [9] propose pseudo-log-polar Fourier transform of points located on nonlinearly growing concentric squares to evaluate DFT in the log-polar coordinate. Sampling at non-integer frequencies suffers from inherent errors due to interpolation. For better approximation of log-polar Fourier transform, Pan *et al.* [13] use multilayer fractional Fourier transform (MLFFT). The number of layers and the sampling rate on the 2-D Cartesian MLFFT grid, however, are adjusted on a trial-and-error basis, and the method is not applicable to log-polar transform.

III. LPFFT Algorithm

For a given block of size $n \times n$, complexity of directly computing DFT in the polar coordinates is $O(n^4)$. Since FFT is defined in the Cartesian system, pseudo-polar Fourier transform (PPFT) [7] is proposed to evaluate 2-D Fourier transform on a pseudo-polar grid, which is approximation of the polar grid and reduces computation complexity to $O(n^2\log n)$.

As shown in Fig. 2, the pseudo-polar grid is divided into basically vertical (BV) and basically horizontal (BH) subsets. The BV subset (black dots in Fig. 2) and BH subset (white dots) are defined as

$$\mathrm{BV}: \begin{cases} \xi_y = \frac{\pi l}{N}, & -N \le l < N \\ \xi_x = \xi_y \cdot \frac{2k}{N}, & -\frac{N}{2} \le k < \frac{N}{2} \end{cases} \quad (5)$$

$$\mathrm{BH}: \begin{cases} \xi_x = \frac{\pi l}{N}, & -N \le l < N \\ \xi_y = \xi_x \cdot \frac{2k}{N}, & -\frac{N}{2} < k \le \frac{N}{2}. \end{cases} \quad (6)$$

LPFFT has two steps: fractional Fourier transform and coordinate conversion. We get the log-polar coordinate system directly from interpolation of the pseudo-polar grid, and therefore LPFFT can be computed on images with the same low complexity and high accuracy as PPFFT.

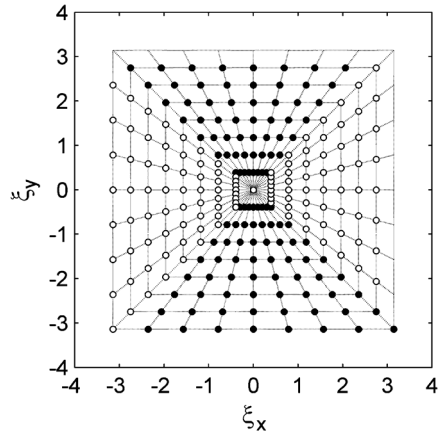

Fig. 2. Pseudo-polar grid and division into BV and BH coordinates ($N = 8$).

A. Fractional Fourier Transform

Fractional Fourier transform (FRFT) [14] is generalization of DFT with computation complexity $O(n\log n)$ instead of $O(n^2)$ of DFT. It evaluates Fourier transform of a sequence $\mathbf{X}$ on an equally spaced set of d points on the unit circle. Given a sequence $\mathbf{X} = (x_j, 0 \le j < d)$ and an arbitrary $\alpha \in \mathbf{R}$, FRFT is

$$F_k(x,\alpha) = \sum_{j=0}^{n-1} x_j \exp(-2\pi jk\alpha), \quad k = 0,\ldots,n-1. \quad (7)$$

Computation of fractional Fourier transform is based on pseudo-polar grid. For BV points, we compute FFT on each column of the points and FRFT on each row of the points with $\alpha = 2k/d$, where k is an index of the row. For BH points, we repeat the same steps for a transposed version of the image.

B. From Pseudo-Polar to Log-Polar

Based on the pseudo-polar grid, we define the log-polar grid that is also divided into the BV and BH subsets:

$$P_{\mathbf{BV}} = \begin{cases} \rho_y = \frac{\pi}{R(k)}\lambda^{\left(\frac{l}{N}-1\right)\pi}, & -N \le l < N \\ \rho_x = \frac{\pi}{R(k)}\lambda^{\left(\frac{l}{N}-1\right)\pi} \cdot \tan\left(\frac{\pi k}{2N}\right), & -\frac{N}{2} \le k < \frac{N}{2} \end{cases} \quad (8)$$

$$P_{\mathbf{BH}} = \begin{cases} \rho_x = \frac{\pi}{R(k)}\lambda^{\left(\frac{l}{N}-1\right)\pi}, & -N \le l < N \\ \rho_y = \frac{\pi}{R(k)}\lambda^{\left(\frac{l}{N}-1\right)\pi} \cdot \tan\left(\frac{\pi k}{2N}\right), & -\frac{N}{2} \le k < \frac{N}{2} \end{cases} \quad (9)$$

where

$$R(k) = \sqrt{1 + \tan^2\left(\frac{\pi k}{2N}\right)}. \quad (10)$$

Samples near the center of log-polar grid are denser than those in the outer region. The parameter λ is used to adjust the different sample density from the center to the edge. For $N = 8$, we find that $\lambda \in [2,3]$ can produce satisfactory accuracy without over-sampling in the center region. In this work, we let $\lambda = 2.5$. The grid conversion takes two steps.

1) To interpolate frequency samples in the BV subset to a log-polar grid, we first rotate the sampling radial lines since the log-polar coordinates require equal-angular spacing. This is done by replacing $2k/N$ in ξ_x of (5) with

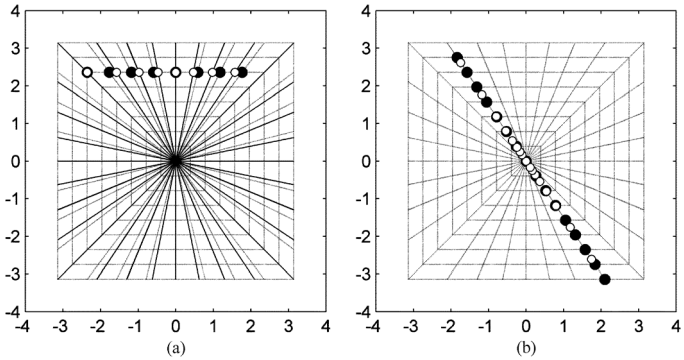

Fig. 3. Interpolation from pseudo-polar grid to log-polar grid ($N = 8$).

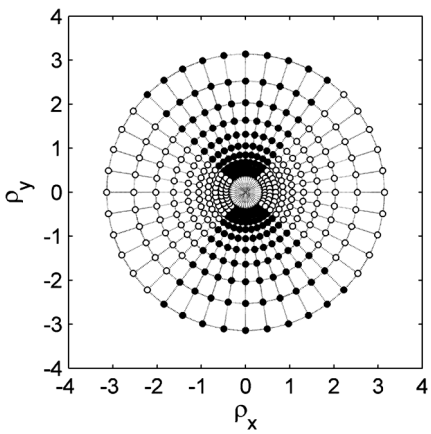

Fig. 4. Log-polar grid with 8 concentric circles and 16 angularly equispaced radial lines.

$\tan(\pi k/2N)$. Fig. 3(a) shows the procedure schematically. Rotating the radial lines relocates a set of N equispaced black dots on the concentric squares to the white dots that are equiangular.

2) Next, we calculate the sample values on the concentric circles with nonlinear increments required by log-polar coordinates. To do so, we replace the term l/N in ξ_y of (5) with $\lambda^{\pi(l/N-1)}$ and divide ρ_y and ρ_x by $R(k)$, as shown in Fig. 3(b). The procedure of interpolating BH samples is the same. Thus, we get the log-polar grid (Fig. 4).

As computation complexity of LPFFT for both BV and BH points are $O(n^2 \log n)$, the overall complexity of LPFFT is also $O(n^2 \log n)$. Pseudo-polar grid points are located at the desired intersection between the linearly growing concentric squares and non-equiangular radial lines, ensuring better accuracy compared to computing FFT directly on the Cartesian grid. Table I gives performance comparison of LPFFT proposed in this paper with LPFT ([6], [16]), FMT ([4]) and PPFFT ([7]). Although [4] and [16] project 2-D log-polar descriptor onto a 1-D descriptor so that the complexity is reduced, this would lead to some limitation of those methods. For example, the algorithm in [4] can only detect forgery with rotation less than 10°, and that in [16] cannot detect forgery of small size.

C. Region Duplication Forgery Detection

It is reasonable to assume that image forgery is performed on image regions with rich contents. Therefore, we skip image regions that lack textures and have few details (e.g., the sky) before detection in order to speed up the detection process and reduce false alarm. The following are steps for detecting image region duplication.

1) Divide an $m \times n$ image $\mathbf{I}$ into $K_0 = (m-d+1)(n-d+1)$ square blocks sized $d \times d$. After removing blocks lacking textures and details, there are K blocks left for detection.
2) Compute LPFFT of each block, including FRFT and grid conversion. The results are denoted as $\{\mathbf{V}_1, \mathbf{V}_2, \ldots, \mathbf{V}_K\}$.
3) Compute normalized cross power spectrum $G(u,v)$ between each pair of $\mathbf{V}_k$, and inverse Fourier transform $\mathcal{F}_G^{-1}(u,v)$ of each $G(u,v)$, resulting in $L = K \times (K-1)/2$ maximal values $\{p_1, p_2, \ldots, p_L\}$, each corresponding to a pair of circles in $\mathbf{I}$.
4) Compare the members in $\{p_1, p_2, \ldots, p_L\}$ with a threshold T chosen as the average absolute value of $\mathcal{F}_G^{-1}(u,v)$. If $p_l (l = 1, 2, \ldots, L)$ is greater than T, the two blocks in $\mathbf{I}$ are regarded as belonging to duplicated regions.

Although LPFFT allows smaller blocks than LPFT, the best choice of block size d is related to the size of tampered regions. Without any *a priori* knowledge of the forgery, we choose the value of d according to the image size. In this work, we let $d = 8$ pixels, giving an acceptable tradeoff between false alarm and detection rates in the experiments. Accordingly, we let N in (8)–(10) equal 8, same as that used in [7]. Overlapped regions are not considered since repeated detection of the same content in these regions would cause false alarm. Detected isolated blocks are also excluded since they are most likely false alarm. Similar to [15], LPFFT results can also be used to estimate the rotation and scaling parameters.

Without projecting 2-D image block feature onto 1-D feature, our method can detect region duplication with any rotation angle. As to the scaling factor, however, if the image is enlarged, a part of the image in the log-polar domain may be moved out of the display area and another part moved in. It means that scaling with a large factor, e.g., greater than 1.5, introduces too much change of the image content in the log-polar domain, which is not considered in this work.

TABLE I
PERFORMANCE ANALYSIS OF DIFFERENT FEATURES

	LPFT	FMT	PPFFT	LPFFT
Complexity	$O(n^4)$	$O(n^4)$	$O(n^2 \log n)$	$O(n^2 \log n)$
Rotation invariance	Yes	Yes	Yes	Yes
Scaling invariance	Yes	Yes	No	Yes

IV. EXPERIMENTAL RESULTS

According to (4), there is a peak in $\mathcal{F}_G^{-1}(u,v)$ of two image regions if one is a replica of the other. To set the threshold T, we perform a series of tests using different T values from 0.1 to 0.5 with an increment 0.05. An appropriate choice can be found between 0.3 and 0.35. We normalize $\mathcal{F}_G^{-1}(u,v)$ and let $T = 0.35$ in the experiment. If the average value of normalized $\mathcal{F}_G^{-1}(u,v)$ is less than T, a peak value exists and the two corresponding image regions are considered to have similar contents.

Fig. 5(a) and (b) present a case of region duplication with rotation. The tempered region in Fig. 5(b) is rotated by 5° and pasted to another part of the image, and the detection result is

(a) (b) (c)

Fig. 5. Detection of rotated region of leaves: (a) the original, (b) tampered by rotating a region by 5° and pasting to another region, and (c) detection result.

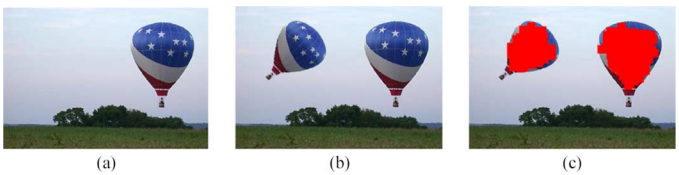

(a) (b) (c)

Fig. 6. Detection of a rotated and scaled balloon: (a) the original, (b) tampered with the balloon rotated by 45° and shrunk by 0.8, and (c) detection result.

(a) (b)

Fig. 7. Detection result of Fig. 1(b): (a) no operation, (b) the tampered image is saved with JPEG quality of 20.

(a) (b) (c)

Fig. 8. Detection of a questionable missile: (a) a picture appeared in many newspapers and websites, (b) an alleged fake image, and (c) detection result.

shown in Fig. 5(c). In Fig. 6, the balloon is duplicated with 45° rotation and a scaling factor 0.8. Fig. 7(a) shows the detection result of Fig. 1(b). The features used are also robust to JPEG compression. Fig. 7(b) is the result when the tampered image is saved with JPEG quality of 20. Fig. 8(b) is an alleged fake image that made headlines in many newspapers and websites in 2008 (http://thelede.blogs.nytimes.com/2008/07/10/in-an-iranian-image-a-missile-too-many/, accessed May 17, 2011). Fig. 8(a) was believed to be taken at about the same time. With the proposed method, two suspicious regions are exposed. The result shows efficacy of the proposed algorithm even when multiple forgeries occur in a single image.

V. Conclusions

We propose an effective method using log-polar fast Fourier transform to detect duplicate image regions that may be rotated and/or re-scaled. The method focuses on low-complexity feature extraction. To speed up the algorithm further, the extracted features should be well organized to fit into computer memory, for example, using lexicographic sorting or counting bloom filters as in [4] and [16]. However, memory optimization is not the topic of this work.

As direct computation of discrete Fourier transform of all blocks is computationally expensive, we have developed a fast algorithm to evaluate discrete Fourier transform in the log-polar domain. The log-polar fast Fourier transform can produce adequate accuracy with much lower computation complexity than the plain LPFT approach. Experimental results are provided to show effectiveness of the method.

References

[1] J. Fridrich, D. Soukal, and J. Lukas, "Detection of copy-move forgery in digital images," in *Proc. Digital Forensic Research Workshop*, Cleveland, OH, 2003.

[2] A. C. Popescu and H. Farid, Exposing Digital Forgeries by Detecting Duplicated Image Regions Dept. Comput. Sci., Dartmouth College, Tech. Rep. TR2004-515, 2004.

[3] M. K. Bashar, K. Noda, N. Ohnishi, and K. Mori, "Exploring duplicated regions in natural images," *IEEE Trans. Image Process.*, vol. 99, 2011, 10.1109/TIP.2010.2046599, Member.

[4] S. Bayram, H. T. Sencar, and N. Memon, "An efficient and robust-method for detecting copy-move forgery," in *Proc. ICASSP*, Taipei, Taiwan, 2009, pp. 1053–1056.

[5] X. Pan and S. Lyu, "Region duplication detection using image feature matching," *IEEE Trans. Inf. Forensics Security*, vol. 5, no. 4, pp. 857–867, Dec. 2010.

[6] Q. Wu, S. Wang, and X. Zhang, "Detection of image region-duplication with rotation and scaling tolerance," in *Proc. 2nd International Conference on Computational Collective Intelligence (ICCCI)*, Kaohsiung, Taiwan, Nov. 10–12, 2010, vol. 6421, Lecture Notes in Computer Science, pp. 100–108.

[7] A. Averbuch, R. R. Coifman, D. L. Donoho, M. Elad, and M. Israeli, "Fast and accurate polar Fourier transform," *Appl. Comput. Harmon. Anal.*, vol. 21, no. 2, pp. 145–167, Sept. 2006.

[8] Y. Keller, A. Averbuch, and M. Israeli, "Pseudopolar-based estimation of large translations, rotations, and scalings in images," *IEEE Trans. Image Process.*, vol. 14, no. 1, pp. 12–22, July 2005.

[9] H. Liu, B. Guo, and Z. Feng, "Pseudo-log-polar Fourier transform for image registration," *IEEE Signal Process. Lett.*, vol. 13, no. 1, pp. 17–20, Jan. 2006.

[10] G. Tzimiropoulos, W. Argyriou, S. Zafeiriou, and T. Stathaki, "Robust FFT-based scale-invariant image registration with image gradients," *IEEE Trans. Patt. Anal. Mach. Intell.*, vol. 32, no. 10, pp. 1899–1906, Oct. 2010.

[11] B. S. Reddy and B. N. Chatterji, "An FFT-based technique for translation, rotation, and scale-invariant image registration," *IEEE Trans. Image Process.*, vol. 5, no. 8, pp. 1266–1271, Aug. 1996.

[12] N. Chou, J. A. Izatt, and S. Farsiu, "Generalized pseudo-polar Fourier grids and applications in registering ophthalmic optical coherence tomography images," in *Proc. 43rd Asilomar Conf. Signals, Systems and Computers*, Nov. 2009, pp. 807–811.

[13] W. Pan, K. Qin, and Y. Chen, "An adaptable-multilayer fractional Fourier transform approach for image registration," *IEEE Trans. Patt. Anal. Mach. Intell.*, vol. 31, no. 3, pp. 400–413, 2009.

[14] D. H. Bailey and P. N. Swarztrauber, "The fractional Fourier transform and applications," *SIAM Rev.*, vol. 33, no. 3, pp. 389–404, 1995.

[15] Y. Keller, Y. Shkolnisky, and A. Averbuch, "The angular difference function and its application to image registration," *IEEE Trans. Patt. Anal. Mach. Intell.*, vol. 27, no. 6, pp. 969–976, Jun. 2005.

[16] S. Bravo-Solorio and A. K. Nandi, "Automated detection and localisation of duplicated regions affected by reflection, rotation and scaling in image forensics," *Signal Process.*, 2011, 10.1016/j.sigpro.2011.01.022.